ELSEVIER

Journal of Nuclear Materials 273 (1999) 130–138

journal of nuclear materials

www.elsevier.nl/locate/jnucmat

Effect of strain rate and test temperature on superplasticity of a Zr–2.5 wt% Nb alloy

S.V. Shukla [a], C. Chandrashekharayya [b], R.N. Singh [c], R. Fotedar [c] R. Kishore [c], T.K. Sinha [c], B.P. Kashyap [b,*]

[a] *Department of Mechanical, Materials and Aerospace Engineering, University of Central Florida, Orlando FL 32816, USA*
[b] *Department of Metallurgical Engineering and Materials Science, Indian Institute of Technology, Bombay, Mumbai 400 076, India*
[c] *Metallurgy Division, Bhabha Atomic Research Centre, Mumbai 400 085, India*

Received 27 November 1998; accepted 8 February 1999

Abstract

Tensile specimens of a Zr–2.5 wt% Nb pressure tube alloy were deformed at strain rates ($\dot{\varepsilon}$) of 3.2×10^{-4}–2.9×10^{-2} s^{-1} and test temperatures (T) of 625–800°C to investigate the nature of stress–strain curves and the optimum condition for superplasticity. The maximum ductility of 1384% was obtained at $T = 700$°C and intermediate strain rate of 3.4×10^{-3} s^{-1}. The stress–strain curves were found to exhibit the dominance of flow hardening, especially in the early part of deformation, followed by flow softening. The variation in ductility and flow stress as a function of test condition is explained by the observed microstructural evolution and fracture behavior.

1. Introduction

Superplasticity is the ability of certain polycrystalline materials to exhibit very high elongations of the order of several hundred percent before failure, with or without diffuse necking [1]. Superplasticity in the materials containing fine equiaxed grains ($d \leqslant 10$ μm, where d is the grain size) is obtained at high temperatures when deformed at intermediate strain rates. Under such condition strain rate sensitivity (m) of flow stress, to which ductility is related, is determined to be high ($m \geqslant 0.5$).

Zr–2.5 wt% Nb (hereafter referred as Zr–2.5Nb) alloy is a material used for pressure tubes in Pressurized Heavy Water Reactors (PHWR). Recently, this material has been shown [2–5] to be superplastic when deformed in the two-phase (α and β) region. However, there appears a wide variation in the values of maximum ductility reported by different investigators. As such not many systematic studies have appeared towards examining the conditions of strain rate and test temperature for optimum superplasticity in this material. In view of this, the aim of the present work on Zr–2.5Nb alloy is: (i) to explore the condition of strain rate and temperature for optimum superplasticity and (ii) to examine the source of variation in ductility in terms of the nature of stress–strain curves, microstructural evolution and failure behaviour.

2. Experimental procedure

Zr–2.5Nb alloy used in the present investigation was obtained as a section of 4.4 mm thick pressure tube in the cold rolled and stress relieved condition. Chemical analysis showed the Nb and oxygen contents of 2.54 wt% and 0.1175 wt%, respectively. The current fabrication route of the Zr–2.5Nb pressure tubes develops a duplex microstructure consisting of fine elongated

* Corresponding author. Tel.: 91-22 578 3579; fax: 91-22 578 3480; e-mail: bpk@met.iitb.ernet.in

0022-3115/99/$ – see front matter
PII: S0022-3115(99)00037-9

α-grains surrounded by a grain boundary network of β-Zr phase [4].

Tensile specimens were machined such that the tensile axis was parallel to the rolling direction. The gauge dimensions were 11.5 mm in length, 4.3 mm in width and 4.4 mm in thickness. Tensile tests were done with an Instron Universal Testing Machine employing constant cross-head speeds. Prior to straining, 30 min were given for preheating to and soaking at the test temperature. The test temperatures were controlled within the accuracy of ±3°C. In order to avoid oxidation during testing, the specimens were coated with borax glass powder, and the tests were performed under the flow of argon. Upon completion of tensile tests, the specimens were quenched in water to freeze the microstructure developed in the course of testing.

Metallographic samples were mechanically polished. Etching was done by immersing the specimens for 5–10 s in the mixture of 50 H_2O:45 HNO_3:5 HF. Grain (phase) size was measured from the optical micrographs by the mean linear intercept method. More than 800 intercepts were considered for each average grain size reported here. No distinction was made between the α- and β-phases for this purpose. The error in the average grain size was within ±0.3 μm at the confidence level of 95%. Fracture surfaces were examined by a JEOL, JSM-840A scanning electron microscope.

3. Results

3.1. Tensile behaviour

3.1.1. Effect of strain rate

Separate tensile specimens were deformed at five nominal strain rates in the range 3.2×10^{-4}–2.9×10^{-2} s^{-1}, but at a constant temperature of 700°C. True stress (σ)–true strain (ϵ) curves from these tests are presented in Fig. 1. As expected, the flow stress is seen to increase with strain rate. Also, instead of a steady state, the flow stress is seen to vary with strain and the nature of stress–strain curve is seen to depend on the imposed strain rate. All the stress–strain curves are found to exhibit flow hardening but the same is replaced by flow softening after some degree of deformation, especially, at higher strain rates. Whereas the rate of flow hardening during the initial part of deformation is seen to increase with strain rate, the rate of flow softening, beyond the peaks in the σ–ϵ curves, is noted to decrease with strain rate. Due to the effects of both the strain rate and strain on flow stress, no unique value of strain rate sensitivity index can be obtained. Instead, the apparent strain rate sensitivity index ($m = \partial \ln \sigma / \partial \ln \dot{\varepsilon}$) was determined from the flow stress values at different strain rates, but at fixed strain levels. The values of m obtained from the slope of $\log(\sigma)$–$\log(\dot{\varepsilon})$ plot, employing regression analysis, were

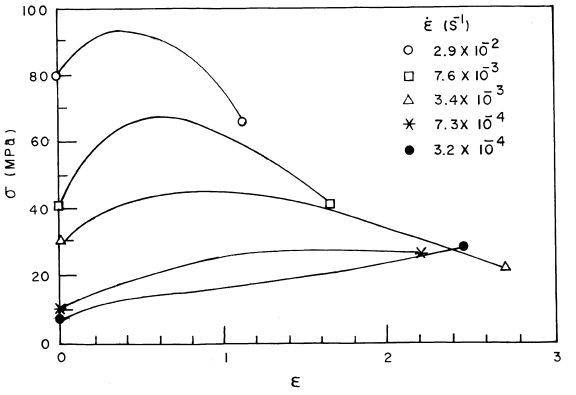

Fig. 1. True stress–true strain curves for Zr–2.5Nb alloy at a constant temperature of 700°C and various constant initial strain rates.

found to decrease with increase in strain as illustrated in Fig. 2. It is seen to follow a bi-linear relationship with a discrete change in slope around $\epsilon \sim 0.70$.

The plot of ductility as a function of initial strain rate, Fig. 3(a), reveals a maximum over a narrow strain rate range in the intermediate region. The maximum ductility of 1384% was obtained at $\dot{\varepsilon} = 3.4 \times 10^{-3}$ s^{-1} whereas the ductility was found to be reduced substantially towards both the lower and higher strain rates. It may be pointed out here that the ductility value corresponding to $\dot{\varepsilon} = 1 \times 10^{-4}$ s^{-1} is taken from Ref. [6]. The silhouette of tensile specimens given in Fig. 3(b) exhibits somewhat sharp necking at the highest strain rate but a reasonably uniform deformation or diffused necking at lower strain rates.

3.1.2. Effect of temperature

Separate tensile specimens were deformed to failure at constant temperatures in the range 625–800°C and at $\dot{\varepsilon} = 2.9 \times 10^{-4}$ s^{-1}. The σ–ϵ curves are presented in Fig. 4. With the decreasing test temperature, the nature of the σ–ϵ curve is noted to change similar to what results with increasing strain rate in Fig. 1. Also, similar to

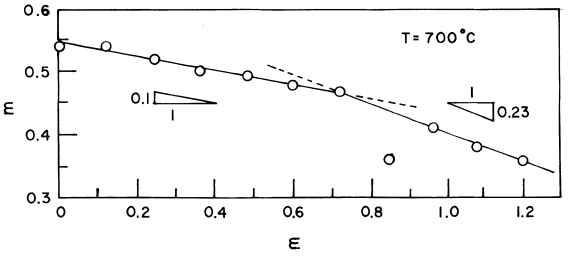

Fig. 2. Variation in strain rate sensitivity index as a function of strain, calculated from the stress–strain curves at various strain rates given in Fig. 1.

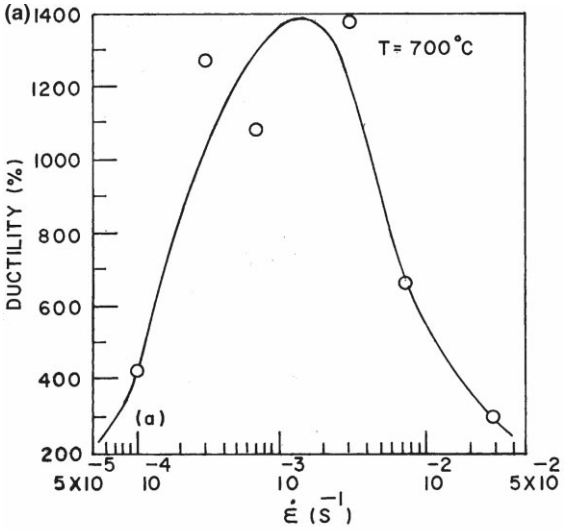

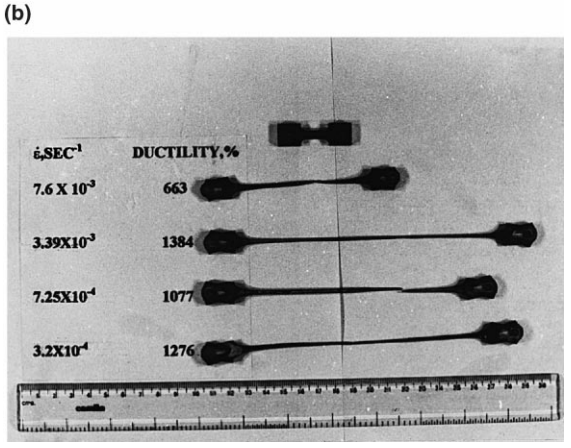

Fig. 3. (a) Effect of initial strain rate on ductility of Zr–2.5Nb alloy at $T = 700$°C. (b) Silhouette of the Zr–2.5Nb tensile specimens deformed to failure at $T = 700$°C and various constant initial strain rates. The specimen at the top is undeformed one for comparison.

the effect of strain rate on ductility, the maximum in ductility was obtained at intermediate temperatures as shown in Fig. 5(a). The maximum ductility obtained was 1350% at 750°C. Silhouette of specimens in Fig. 5(b) again reveals necking towards lower temperatures but uniform deformation towards higher temperatures.

3.2. Microstructural evolution

The microstructure of as-received Zr-2.5Nb alloy consisted of α-grains surrounded by β-phase network, where α and β, respectively represent solid solutions of Nb in hcp and bcc crystal structure of Zr. As reported earlier [4], typical dimensions of α-grains were ~15–20

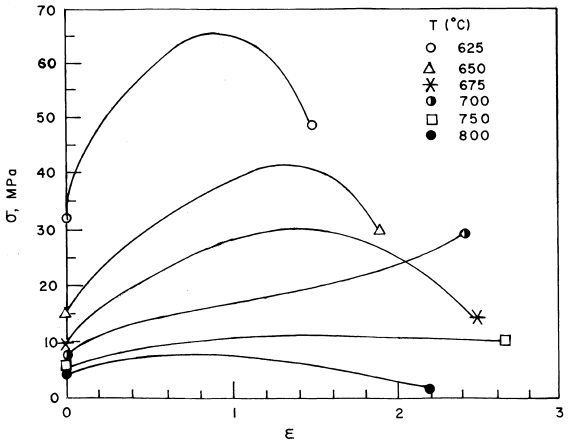

Fig. 4. True stress–true strain curves for Zr–2.5Nb alloy at $\dot{\varepsilon} = 2.9 \times 10^{-4}$ s^{-1} and various constant test temperatures.

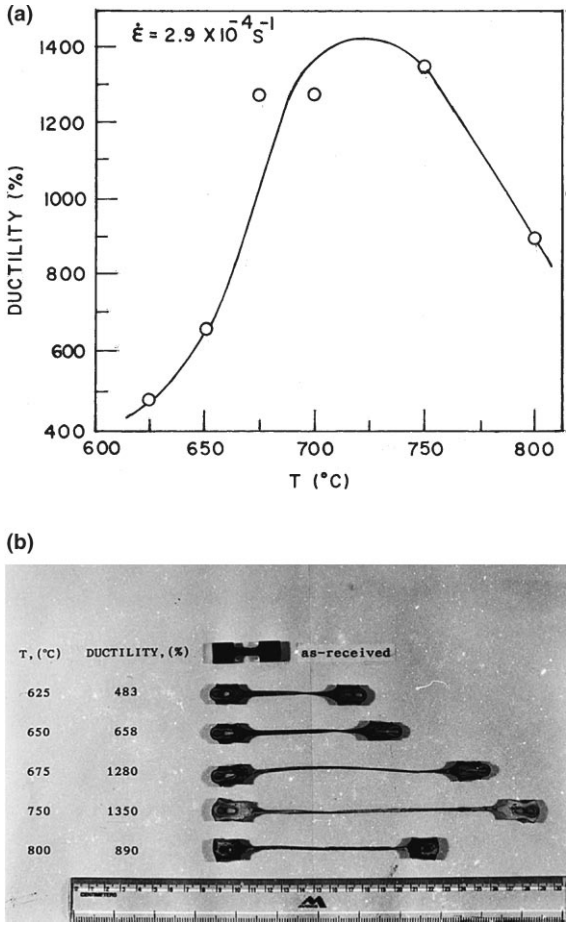

Fig. 5. (a) Effect of test temperature on ductility of Zr–2.5Nb alloy at $\dot{\varepsilon} = 2.9 \times 10^{-4}$ s^{-1}. (b) Silhouette of the Zr–2.5Nb tensile specimens at the initial strain rate of 2.9×10^{-4} s^{-1} and various constant test temperatures. The specimen at the top is undeformed one for comparison.

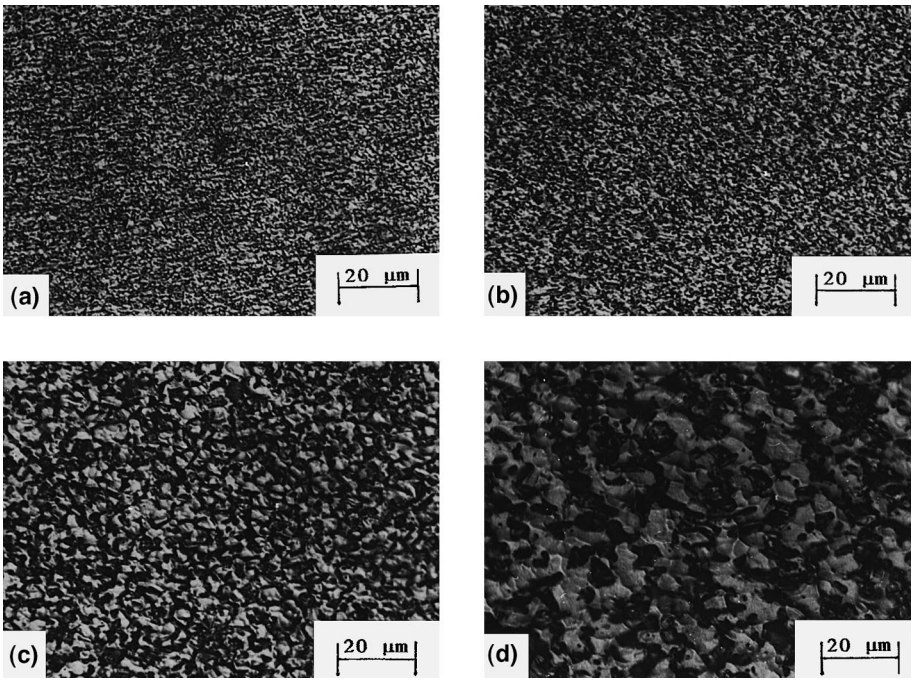

Fig. 6. Microstructures of the shoulder (a,c) and gauge (b,d) sections of the Zr–2.5Nb alloy specimens deformed to failure at $T = 700°C$ but at different strain rates: (a,b) $\dot{\varepsilon} = 2.9 \times 10^{-2}$ s^{-1}, (c,d) $\dot{\varepsilon} = 3.2 \times 10^{-4}$ s^{-1}.

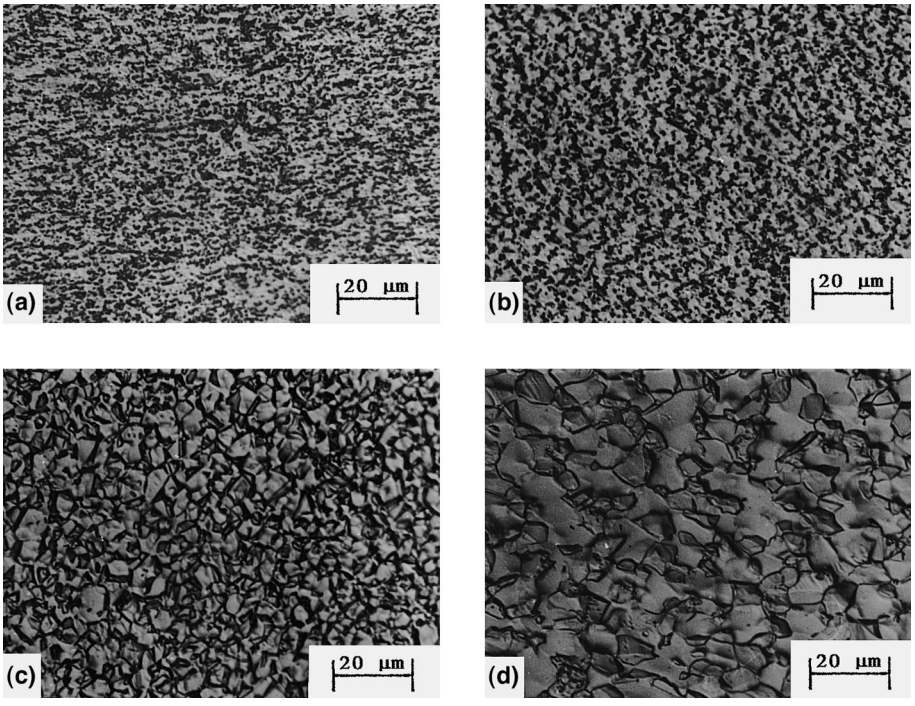

Fig. 7. Microstructures of the shoulder (a,c) and gauge (b,d) sections of the Zr–2.5Nb alloy specimens deformed to failure at $\dot{\varepsilon} = 2.9 \times 10^{-4}$ s^{-1} but at different test temperatures: (a,b) $T = 625°C$, (c,d) $T = 750°C$.

μm × 3–4 μm × 0.25–0.35 μm in length (axial), width (Circumferential) and thickness (radial), respectively. Upon deformation at high temperatures (625–800°C), followed by rapid quenching to room temperature, the β-phase was found to undergo martensitic transformation into α′-phase while α-phase remained untransformed. The subsequent etching process revealed the β-phase as 'dark' and α-phase as 'bright'.

Grain sizes in the shoulder and gauge sections of all the tensile specimens, deformed to failure, were measured. The grain sizes obtained as a function of strain rate and test temperature are listed in Table 1. Also included in Table 1 are the values of ductility obtained under different test conditions. The microstructures in the shoulder and gauge sections of all the specimens were found to be equiaxed, except that some degree of grain elongation was retained in shoulder sections of the specimens deformed at the highest strain rate ($\dot{\varepsilon} = 2.9 \times 10^{-2}$ s^{-1}) or lowest test temperature ($T = 625$°C). Irrespective of strain rate and test temperature, the grain sizes were measured to be larger in the gauge sections than that in the shoulder sections, Table 1. Some typical micrographs of the shoulder and gauge sections, following tensile tests, are presented in Figs. 6 and 7 to illustrate the effects of strain rate (Fig. 6) and test temperature (Fig. 7). The grain sizes in both the shoulder and gauge sections, as well as the difference between the two grain sizes, were found to increase with the decrease in strain rate. With the increase in test temperature, however, the shoulder and gauge sections of the specimens were found to exhibit the largest grain sizes when deformed at intermediate temperatures. Since the magnitude of ductility was found to vary with strain rate and test temperature, the comparison of grain growth was made after normalizing by ductility. For this purpose, the grain sizes of the shoulder section (d_s) was subtracted from the grain sizes of the respective gauge sections (d_g) and the difference was divided by ductility (D), (i.e. $(d_g - d_s)/D$). In this case also the effect of strain rate and temperature was similar to what has already been described above. Fig. 8 shows the effect of strain rate on such a normalized grain growth at 700°C.

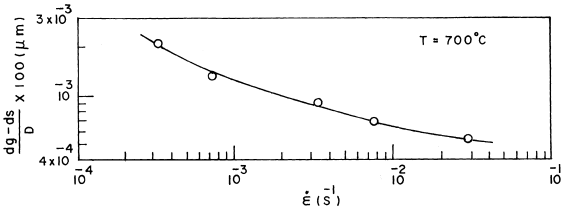

Fig. 8. Plot of deformation induced grain growth normalized by elongation to failure vs strain rate.

3.3. Fractography

Fracture surfaces of the specimens deformed to failure under different conditions were examined. At low magnifications the fracture surfaces appeared to be featureless, supporting the occurrence of pseudo-brittle type failure. With the increase in test temperature, however, there appeared some tearing, cavitation and cracks as shown in Fig. 9(a)–(c). The specimen deformed at the highest temperature of 800°C and the strain rate of 2.9×10^{-4} s^{-1} was noted to exhibit classical chisel fracture, as shown in Fig. 9(c). Fig. 9(c) also reveals intergranular and transgranular cracks. The intergranular cracks are found to be associated with r-type (spherical) voids along the grain boundaries and w-type (wedgelike) cracks at triple points.

Some typical fractographs at higher magnifications are presented in Fig. 10, where a large number of parallel or mutually intersecting cracks are visible. The comparison of fractographs of the specimens deformed at different conditions suggests an increase in the density of cracks with the increase in temperature (Fig. 10(c)–(e)) and decrease in strain rate (Fig. 10(a) and (b)). There also appears some evidence of oxidation on fracture surfaces with the oxide particles disbursed as

Table 1
Data of final grain sizes (μm) in the shoulder and gauge sections of the Zr–2.5Nb alloy specimens deformed at: (a) $T = 700$°C and various initial strain rates, (b) $\dot{\varepsilon} = 2.9 \times 10^{-4}$ s^{-1} and different test temperatures

(a) Effect of strain rate ($\dot{\varepsilon}$, s^{-1}) at $T = 700$°C					
varepsilon	2.9×10^{-2}	7.6×10^{-3}	3.4×10^{-3}	7.3×10^{-4}	3.2×10^{-4}
Ductility (%)	300	663	1384	1077	1276
Shoulder	1.56	2.00	2.00	2.16	2.81
Gauge	1.73	2.46	3.24	3.56	5.46

(b) Effect of temperature (T, °C) at $\dot{\varepsilon} = 2.9 \times 10^{-4}$ s^{-1}						
T	625	650	675	700	750	800
Ductility (%)	483	658	1280	1276	1350	890
Shoulder	1.82	1.98	2.24	2.81	3.63	2.56
Gauge	2.45	3.23	3.60	5.46	4.98	3.91

dispersoids in the valleys or at the origins of such cracks, Fig. 10.

4. Discussion

4.1. Nature of stress–strain curves

Stress–strain curves, presented in Figs. 1 and 4, show flow hardening during the initial part of deformation which is followed by flow softening, except towards the lower strain rates and intermediate temperatures where only flow hardening is noted to prevail up to failure. The strain corresponding to the peak stress, at which the transition from flow hardening to flow softening occurs, is noted to decrease with the increase in strain rate (Fig. 1) and the decrease in test temperature (Fig. 4), In conventional materials, the flow hardening part is ascribed to dynamic recovery process whereas flow softening is ascribed to dynamic recrystallization during high temperature deformation [7]. Under this condition, the strain associated with the peak stress is known to increase with the increase in strain rate and decrease in test temperature [7]. As noted from Figs. 1 and 4, the effects of strain rate and test temperature are exactly opposite to this trend. It may be pointed out that an apparent transition in flow behaviour can also be present as a consequence of the early onset of necking, in which case the true stress determination, under the assumption of uniform deformation, becomes inapplicable.

In superplastic materials, flow hardening is attributed to grain growth whereas flow softening is attributed to dynamic recrystallization or breaking up of the initial elongated grains into equiaxed grains [8]. In the strain rate sensitive materials, an apparent flow softening also results due to continuous decrease in strain rate with the progress in deformation at constant cross-head speed, instead of constant true strain rate. The initial microstructure of the as-received Zr–2.5Nb alloy, investigated here showed highly elongated α-grains having grain aspect ratio as high as 5. Such microstructure undergoes simultaneous grain growth and evolution towards equiaxed grains. Then the flow stress is reflected as the effect of the one which dominates between the two. Although the grain size was not measured as a function of strain in the present study, grain growth normalized by ductility in Fig. 8 suggests it to be maximum at the lowest strain rate. A similar trend was reported in several other superplastic materials [9]. In view of this, the flow hardening at lower strain rates may be the result of concomitant grain growth. By evaluating quantitatively the effect of concurrent grain growth on flow stress, Kashyap and Tangri [10] noted that grain growth could account for flow hardening satisfactorily only at lower strain rates and higher temperatures. The flow hardening at higher strain rates and relatively lower

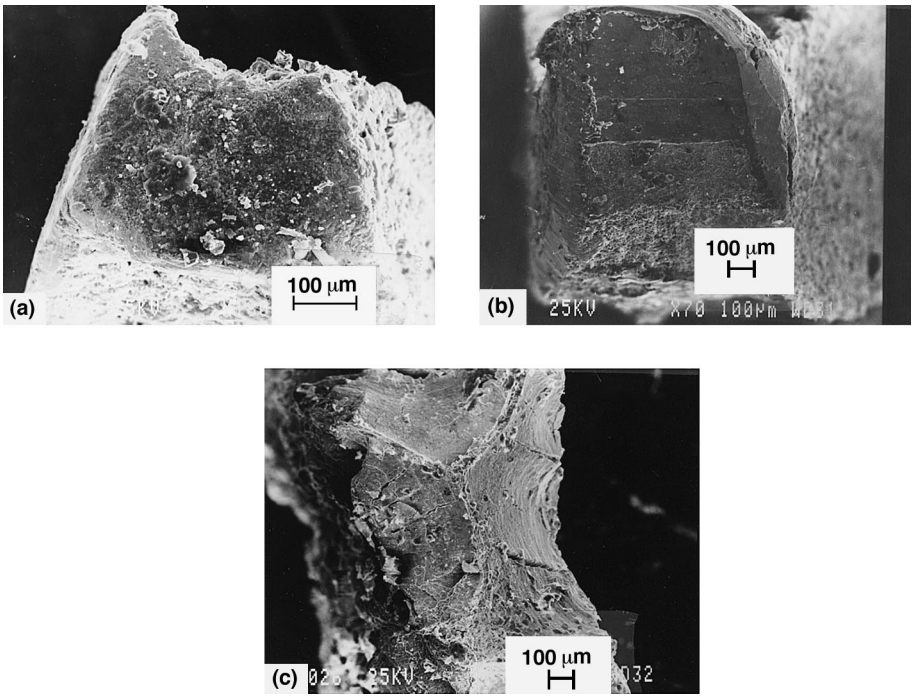

Fig. 9. Fractographs of Zr–2.5Nb alloy specimens tested in superplastic regime at: (a), $T = 700°C$, $\dot{\varepsilon} = 7.6 \times 10^{-3}$ s^{-1}; (b), $T = 625°C$, $\dot{\varepsilon} = 2.9 \times 10^{-4}$ s^{-1}; (c), $T = 800°C$, $\dot{\varepsilon} = 2.9 \times 10^{-4}$ s^{-1}.

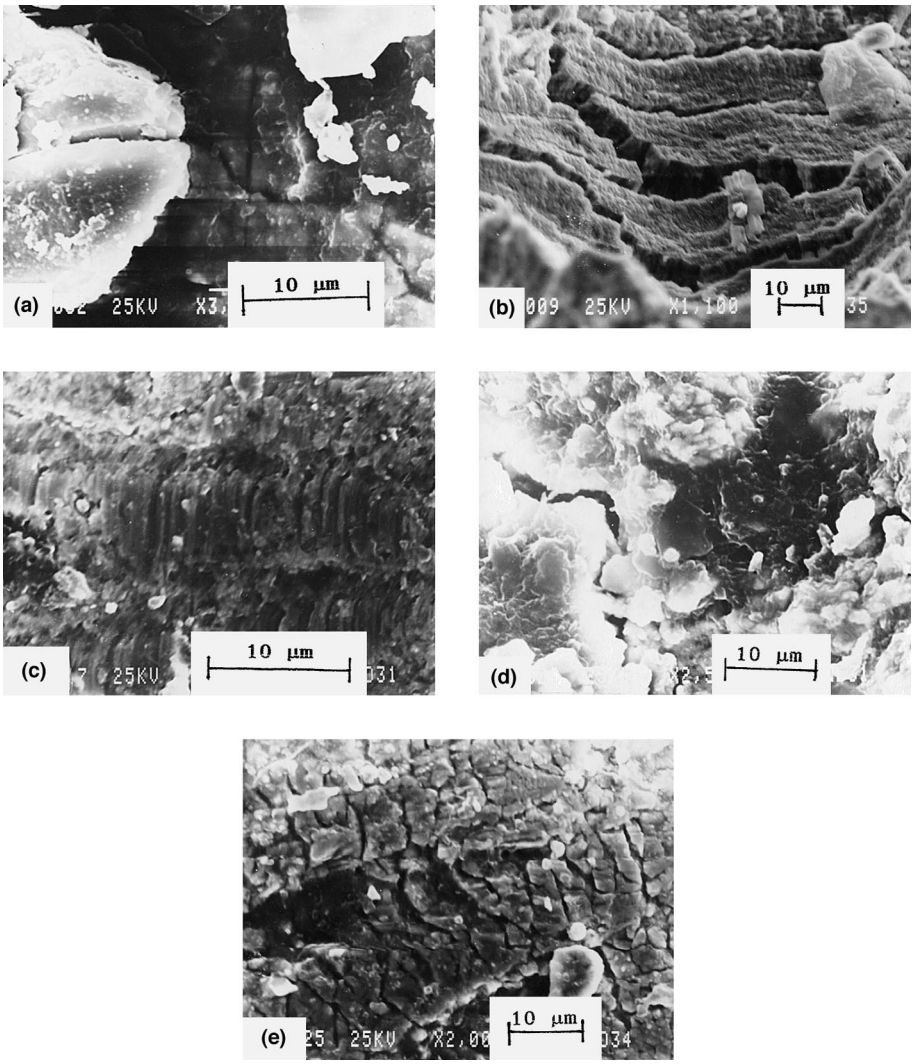

Fig. 10. Some typical fractographs, at high magnifications, of Zr–2.5Nb alloy specimens tested in superplastic regime at: (a), $T = 700°C$, $\dot{\varepsilon} = 7.6 \times 10^{-3}$ s^{-1}; (b), $T = 700°C$, $\dot{\varepsilon} = 7.3 \times 10^{-4}$ s^{-1}; (c), $T = 625°C$, $\dot{\varepsilon} = 2.9 \times 10^{-4}$ s^{-1}; (d), $T = 650°C$, $\dot{\varepsilon} = 2.9 \times 10^{-4}$ s^{-1}; (e), $T = 750°C$; $\dot{\varepsilon} = 2.9 \times 10^{-4}$ s^{-1}.

temperatures, on the other hand, was ascribed to dislocation activity. This may also be the case here since the rate of flow hardening is noted to increase at higher strain rates (Fig. 1) and lower temperatures (Fig. 4) whereas the grain growth follows the opposite trend. The reason for flow softening is not evident at present because the microstructures after heating to and soaking at the test temperatures, prior to deformation, appear to have become nearly equiaxed. For example, see Fig. 6(a) which is found to exhibit a much smaller grain aspect ratio in comparison to that of the as-received material, which exhibited larger grain aspect ratio of ~5. In the absence of grain size data before and immediately after the peak in stress–strain curves, it is also not possible to ascribe the flow softening to dynamic recrystallization. The final grain sizes obtained here only show grain growth rather than a decrease in grain size; it does not bring out if the grain size ever decreased in the course of deformation to support the occurrence of dynamic recrystallization.

4.2. Variation in ductility

The ductility vs strain rate (initial) plot in Fig. 3(a) shows the maximum ductility at intermediate but narrow strain rate range around 2×10^{-3} s^{-1}, above or below which ductility reduces rapidly. In the superplasticity literature e.g., [11], such a variation in ductility is ascribed to the analogous variation of m as a function of (log) strain rate. The variation in ductility of the Zr–2.5Nb

alloy is also supported by the similar variation in m value as a function of initial strain rate at $T = 700°C$ [4]. Since, the greater value of m provides more resistance to necking during superplastic deformation, the maximum ductility is obtained in the intermediate strain rate range.

The variation in ductility as a function of test temperature (Fig. 5(a)) is noted to be similar to its variation with strain rate i.e., there is a maximum in ductility both at intermediate strain rates and intermediate temperatures, within the two-phase region of this alloy. Such a variation in ductility as a function of temperature can be explained by an analogous effect of temperature on m, as reported by Makhutov et al [3]. The reasons for such a variation in ductility and m as a function of temperature are suggested below. First, it is to be noted that the equiaxed microstructure is present in the gauge section of the Zr–2.5Nb tensile specimens even after a large amount of deformation (Figs. 6 and 7). This suggests grain boundary sliding (GBS) to be the dominant deformation process. In order to get a large ductility, it is essential to relieve the stress concentration created by the GBS process. This can be achieved by an increased diffusivity as a result of the increase in test temperature. The first part of the curve, exhibiting the increase in ductility with the increasing test temperature in Fig. 5(a), can thus be understood. The latter part of the curve, viz., the decrease in ductility with the further increase in temperature, can be understood as follows. The magnitudes of GBS and grain growth in two-phase materials, which can influence ductility, depend on the volume fractions of the constituent phases. Grain boundary sliding in α/α, β/β and α/β boundaries are known to be different in α/β brass [12], Pb–Sn eutectic [13] and Zn–Al eutectoid [14]. With the increase in temperature, in the two-phase region for Zr–2.5Nb alloy, the proportion of β phase increases at the expense of α phase. If the different types of interfaces in this alloy also show a variation in GBS then the contribution of GBS to total strain is expected to be maximum for an optimum proportion of the two phases. Also, the presence of second phase restricts grain growth, but the extent to which it is effective depends on its volume fraction and size. According to the effect of phase proportion on grain growth, investigated earlier in another system [15], the increasing volume fraction of β phase with temperature can cause a reduction in the size of α phase but an increase in the size of β phase. Thus, under the content of intermediate phase proportions, which should coincide with some intermediate temperatures, both the phases are likely to possess fine grains. Therefore, at intermediate temperatures, the proportion of the two phases could be optimum for grain boundary sliding and the inhibition of grain growth, which could lead to a maximum in ductility. As the temperature increases beyond the optimum temperature the proportion of α and β phases will become less favorable for GBS and grain growth inhibition, leading to a reduction in ductility with the increase in test temperature.

4.3. Fracture behavior

Superplastic materials generally exhibit four distinct types of fracture: (i) fracture by quasi-stable plastic flow, (ii) failure by necking, (iii) cavitation failure, and (iv) quasi-brittle failure [16]. Maximum elongation occurs when the specimen pulls out to a fine wire in quasi-stable flow. Except at relatively lower temperatures and higher strain rates, tensile specimens in the present work failed in a pseudo-brittle manner, without undergoing substantial necking (Fig. 3(b) and Fig. 5(b)). Unlike many superplastic materials, which exhibit the extensive cavitation to be responsible for pseudo-brittle fracture at high temperature [17], the Zr–2.5Nb alloy exhibited extensive cracking. As seen in Fig. 9(c), these cracks are associated with the voids formed at grain boundaries and triple points. While the voids along the grain boundaries are r-type voids, those at the triple points are w-type voids. Such voids are nucleated as a result of stress concentration built up by GBS and the inability to accommodate the same at the obstacles. The formation of r- and w-type voids depends on the stress level which, in turn, depends on test condition and microstructure. While the r-type voids predominantly form with the decrease in stress and grain size, w-type voids form under opposite conditions [18]. Owing to extensive grain boundary sliding, and sometimes the same in a co-operative manner, during superplastic deformation [19,20], both types of voids can nucleate but they appear to have transformed into cracks without going through the conventionally large growth and coalescence.

Fractographs presented in Fig. 10 reveal some unusual features of distinct, periodic crack front markings and repetitive fissures that appear to be quite deep (Fig. 10(b)), beach mark striations with superimposed fissures (Fig. 10(c)), mud crack pattern (Fig. 10(a),(d)) and network of cracks (Fig. 10(e)). Such features are commonly found in fatigue fracture and intergranular corrosion rather than in conventional tensile tests. While oxidation, in spite of the precautions taken here, can be understood to result in intergranular stress corrosion, it is hard to explain the existence of striations at this stage. Probably, these abnormal features may have their origin in the deformation-environment interactions during the progress in superplastic straining.

5. Conclusions

Investigation on the nature of stress–strain curves and microstructural examination of the Zr–2.5Nb alloy leads to the following conclusions.

1. As-received elongated microstructure changes towards equiaxed grains with concurrent grain growth to varying extent. Grain growth and the conventional strain hardening are suggested to govern the nature of flow curves over a wide range of conditions.
2. The Zr–2.5Nb alloy exhibits maximum elongations of 1384% and 1350% when deformed at 700°C at the initial strain rate of 1×10^{-3} s^{-1} and at 725°C at the initial strain rate of 2.9×10^{-4} s^{-1}, respectively. Ductility is limited by a reduction in the value of m with increasing strain.
3. Fracture surfaces are found to reveal the predominance of cracks with limited cavities. Under the optimum conditions of superplasticity, there occurs cavitation whereas under other conditions the cracks are seen to be more predominant.

Acknowledgements

This work was financially supported under the grant # 34/8/93-G/429 and permitted for publication by the Board of Research in Nuclear Science of India. The authors are grateful to Dr S. Banerjee for encouragement and help. The authors also thank Professor P.K. Saraswati and Ms Rupali Samant for their help in scanning electron microscopy.

References

[1] K.A. Padmanabhan, G.J. Davis, Superplasticity, Springer, Berlin, New York, 1980.
[2] K. Nuttall, Scripta Metall. 10 (1976) 835.
[3] N.A. Makhutov, L.P. Fedorovich, Aa.V. Chirkin, B.G. Parfenov, A.I Tanenov, Met. Sci. Heat Treat. 24 (1982) 491.
[4] R.N. Singh, R. Kishore, T.K. Sinha, B.P. Kashyap, Scripta Metall. Mater. 28 (1993) 937.
[5] R.N. Singh, R. Kishore, T.K. Sinha, B.P. Kashyap in: Atul Chokshi (Ed.), Superplasticity in Advanced Materials ICSAM-97, Proceedings of the 1997 International Conference, Banglore, India, Trans Tech publication, Materials Science Forum, 1997, vols. 243–245, p. 499.
[6] Akash, thesis, Indian Institute of Technology, Mumbai, India, 1994.
[7] H.J. McQueen, J.J. Jonas, in: Treatise in Materials Science and Technology, vol. 6, Plastic Deformation of Materials, Academic Press, San Francisco, 1975, p. 393.
[8] M. Suery, B. Baudelet, Rev. Phy. Appl. 13 (1978) 53.
[9] D.S. Wilkinson, C.H. Caceres, J. Mater. Sci. Lett. 3 (1984) 395.
[10] B.P. Kashyap, K. Tangri, Metall. Trans. 18A (1987) 417.
[11] T.G. Langdon, Metall. Trans. 13A (1982) 689.
[12] T. Chandra, J.J. Jonas, D.M.R. Taplin, J. Mater. Sci. 13 (1978) 2380.
[13] R.B. Vastava, T.G. Langdon, Acta Metall. 27 (1979) 251.
[14] P. Shariat, R.B. Vastava, T.G. Langdon, Acta Metall. 30 (1982) 285.
[15] P.K. Bakshi, B.P. Kashyap, J. Mater. Sci. 29 (1994) 2063.
[16] T.G. Langdon, Met. Sci. 16 (1982) 175.
[17] B.P. Kashyap, A.K. Mukherjee, Res. Mechan. 17 (1986) 293.
[18] Thomas H. Courtney: Mechanical Behavior of Materials, McGraw-Hill, New York, 1990.
[19] B.P. Kashyap, A.K. Mukherjee, J. Mater. Sci. 20 (1985) 2661.
[20] O.A. Kaibyshev, A.I. Pshenichnyuk, V.V. Astanin, Acta Mater. 46 (1998) 4911.